



University  
of Glasgow

Fulda, P., Bond, C., Brown, D., Brückner, F., Carbone, L., Chelkowski, S., Hild, S., Kokeyama, K., Wang, M., and Freise, A. (2012) *Review of the Laguerre-Gauss mode technology research program at Birmingham*. Journal of Physics: Conference Series, 363 (1). 012010. ISSN 1742-6588

Copyright © 2012 The Authors

<http://eprints.gla.ac.uk/94624/>

Deposited on: 20 June 2014

Enlighten – Research publications by members of the University of Glasgow  
<http://eprints.gla.ac.uk>

# Review of the Laguerre-Gauss mode technology research program at Birmingham

**P. Fulda, C. Bond, D. Brown, F. Brückner L. Carbone, S. Chelkowski<sup>1</sup>, S. Hild<sup>2</sup>, K. Kokeyama<sup>3</sup>, M. Wang, and A. Freise**

School of Physics and Astronomy, University of Birmingham  
Edgbaston, Birmingham, B15 2TT, UK

E-mail: pfulda@star.sr.bham.ac.uk

**Abstract.** Gravitational wave detectors of the advanced generation are expected to be limited in sensitivity by thermal noise of the optics. The reduction of this noise is therefore of high importance for future detectors which aim to surpass the sensitivity of the advanced generation. A proposed method for reducing the impact of this noise is to use higher-order Laguerre-Gauss (LG) modes for the readout beam, as opposed to the currently used fundamental mode. We present here a synopsis of the research program undertaken by the University of Birmingham into the suitability of LG mode technology for future gravitational wave detectors. This will cover our previous and current work on this topic, from initial simulations and table-top LG mode experiments up to implementation in a prototype scale suspended cavity and high-power laser bench.

## 1. Introduction

Advanced gravitational wave detectors such as Advanced LIGO [1] and Advanced Virgo [2] are being constructed with the goal of a tenfold increase in sensitivity over the first generation of detectors [3, 4]. This is expected to be sufficient to make the first conclusive gravitational wave detection. The projected sensitivity of both Advanced LIGO and Advanced Virgo will be limited over the observation frequency band by several fundamental noise sources: seismic noise, radiation pressure noise, suspension thermal noise, shot noise, and thermal noise of the test masses themselves [5]. The dominant contribution to the total thermal noise of the test masses is expected to be from the Brownian motion of the atoms that make up the reflective coatings. This motion causes an uncertainty in the phase of the light reflected from the test mass, and will therefore appear as noise in the detector output. This thermal noise has until now not been a limiting noise source in detectors, but as progress within the field pushes other noise sources ever lower, its mitigation becomes a more urgent priority.

One way to reduce the effects of the coating Brownian thermal noise is to use a larger beam spot on the test mass surfaces, since a larger beam averages more effectively over the random motions of the surface. The coating Brownian thermal noise power spectral density has been

<sup>1</sup> Presently at: Jenoptik AG, Carl-Zeiss-Strasse 1, 07739, Jena, Germany

<sup>2</sup> Presently at: Institute for Gravitational Research, University of Glasgow, G12 8QQ, UK

<sup>3</sup> Presently at: Physics and Astronomy, Louisiana State University, Baton Rouge, LA 70803, USA

shown to scale with the inverse square of the Gaussian beam size parameter  $w(z)$  [6]. However, as the beam spots are made larger, a larger fraction of the light power is lost over the edge of the reflective surface. This fraction is known as the *clipping loss*. If one uses a beam with a more homogeneous radial intensity distribution than the commonly used LG<sub>00</sub> beam, the Brownian thermal noise level can be reduced without increasing the clipping loss. Several beams with this property have been suggested for gravitational wave detectors, including mesa beams [7], optimised conical beams [8] and higher-order LG beams [9].

Higher-order LG modes have the advantage over the other suggested beams of being compatible with spherical mirror surfaces, as currently used with the LG<sub>00</sub> mode. Equation 1 shows the complex amplitude function for the helical higher-order mode set,

$$u_{p,l}^{\text{hel}}(r, \phi, z) = \frac{1}{w(z)} \sqrt{\frac{2p!}{\pi(|l|+p)!}} e^{(2p+|l|+1)\Psi(z)} \times \left(\frac{\sqrt{2}r}{w(z)}\right)^{|l|} L_p^{(|l|)}\left(\frac{2r^2}{w(z)^2}\right) e^{-ik\frac{r^2}{2q(z)}+il\phi}, \quad (1)$$

where  $p$  is the radial mode index,  $l$  is the azimuthal mode index,  $w$  is the beam radius,  $k$  is the wave-number,  $q$  is the complex Gaussian beam parameter,  $L_p^{(|l|)}$  are the associated Laguerre polynomials, and  $\Psi$  is the Gouy phase, given by

$$\Psi(z) = \arctan\left(\frac{\lambda z}{\pi w_0^2}\right). \quad (2)$$

The order of a higher-order LG mode is given by  $2p + |l|$ . An alternative sinusoidal form of LG modes with a sinusoidal amplitude dependence in azimuthal angle can be used equally well. In this article we will discuss the research performed by the Birmingham group towards evaluating the feasibility of LG mode technology for implementation in detectors of the advanced generation and beyond to reduce the test mass thermal noise limit.

## 2. Interferometric performance simulation study of LG modes

Our initial step was to compare the interferometric performance of the LG<sub>33</sub> mode to the LG<sub>00</sub> mode in an optical layout similar to that proposed for the advanced detectors. By interferometric performance we mean the level of coupling of a number of variables to the measured phase ('phase noise analysis'), the ability to generate the required longitudinal and alignment control signals, and finally the maximum achievable detector sensitivity. The first consideration to ensure a fair analysis of the performance of the LG<sub>33</sub> mode was the beam sizes which should be compared. The advanced detectors use larger beam sizes on the test masses than the first generation detectors, irrespective of the spatial mode used, since the limiting Brownian noise level scales with the inverse square of the beam size. The limit on beam size can be enforced either by the point at which the clipping loss becomes unacceptably high, or the point at which cavities become unacceptably close to the unstable concentric design required for maximising beam sizes. For this study we considered the limit to be enforced by the clipping loss, which we fixed at 1 ppm.

The higher-order LG modes are more spatially extended, and thus have larger clipping losses than the LG<sub>00</sub> mode for a given beam spot size parameter. The ratio between LG<sub>00</sub> spot size and LG<sub>33</sub> spot size required to give a 1 ppm clipping loss on the same mirror is  $\frac{w_{00}}{w_{33}} = 1.64$ . In the rest of this section we will compare the performance of three different configurations for a symmetric 3 km cavity, to be referred to as the LG<sub>33</sub>, LG<sub>00</sub><sup>large</sup> and LG<sub>00</sub><sup>small</sup> configurations. The LG<sub>33</sub> and LG<sub>00</sub><sup>large</sup> configurations both have a clipping loss of 1 ppm at the cavity mirrors, thus the beam size at the mirrors for LG<sub>00</sub><sup>large</sup> configuration is factor of 1.64 larger than for the LG<sub>33</sub> configuration. The LG<sub>00</sub><sup>small</sup> configuration has the same spot size at the mirrors as the LG<sub>33</sub> configuration, but uses a LG<sub>00</sub> beam, and therefore has a lower clipping loss. The LG<sub>00</sub><sup>small</sup> configuration is less realistic for comparison with the LG<sub>33</sub>, for the aforementioned reason that

advanced detectors will be pushing towards larger beam sizes irrespective of spatial mode used, but we found it useful to include in the study to separate the effects due beam parameters and effects due directly to mode shape.

The first control signal investigated was the longitudinal error signal for a single cavity. For a Pound-Drever-Hall (PDH) modulation/demodulation error signal generation technique [11], the resulting longitudinal control signal was identical for all three of the considered configurations. The next step was an analysis of the coupling from end mirror tilt to longitudinal phase noise in a single cavity for each configuration. Figure 1 shows the results of the investigation for a 3 km cavity based on the Advanced Virgo reference design in [10]. The  $LG_{00}^{\text{small}}$  configuration performs slightly better than the  $LG_{33}$  here, but of the two configurations with equal clipping losses, the  $LG_{33}$  configuration performs significantly better than the  $LG_{00}^{\text{large}}$  configuration. This is because the  $LG_{00}^{\text{large}}$  configuration requires the cavity to be pushed closer to the unstable concentric design in order to achieve the necessary beam sizes at the mirrors.

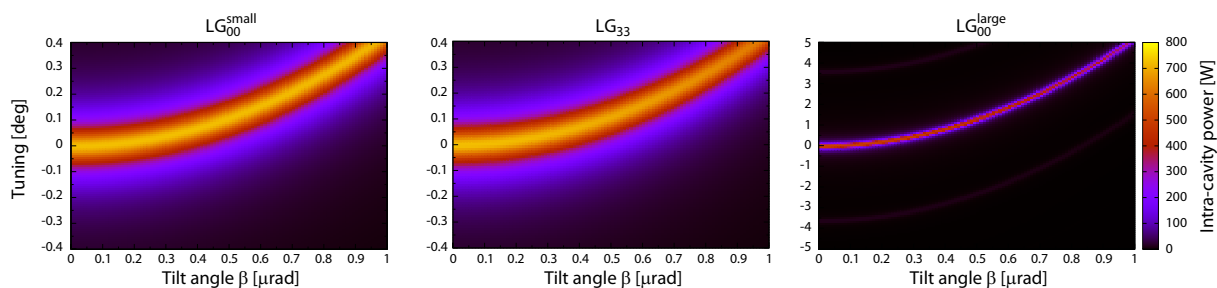


**Figure 1.** Intra cavity power as a function of cavity end mirror tilt angle  $\beta$  and longitudinal tuning  $\phi$  for the three different configurations. The first two configurations show very similar results, but the  $LG_{00}^{\text{large}}$  configuration shows a much stronger coupling from tilt to tuning (note the larger scale on the tuning axis in the  $LG_{00}^{\text{large}}$  plot).

As well as length sensing and control, angular sensing and control is crucial to maintaining stable operation and maximum sensitivity of a gravitational wave interferometer. To investigate how the  $LG_{33}$  mode performs in this respect, an alignment scheme based on the Ward technique described in [12] was designed for the same 3 km cavities previously described. The optical layout for this scheme is shown in panel (A) of figure 2. Radio frequency sidebands are added to the beam by the electro-optic modulator (EOM), and the beam is passed into the cavity via a beam splitter. The reflected beam from the cavity is split in two, and each resulting beam is passed through a telescope and detected with a quadrant photodetector. These telescopes are designed such that the Gouy phase (see equation 2) difference between the beams at each quadrant photodetector is  $90^\circ$ , in order to provide the maximum possible orthogonality between alignment signals from the end mirror and the input mirror. The signal from each photodetector is demodulated by mixing with the initial radio frequency, with a demodulation phase chosen such as to maximise the slope of the error signal corresponding to the mirror for which the photodetector is required to sense the alignment. In order to match the conditions under which the alignment control system will be developed in practice as closely as possible, we tuned the parameters rather than using the theoretical optimum parameters.

The alignment sensing figure of merit for each configuration can be summarized by its control matrix [13]. The elements  $\sigma_{\text{detector}}^{\text{mirror}}$  of these control matrices are the slopes of the error signal at the working point as measured at quadrant photodetectors QPD1 and QPD2, for misalignments of the cavity input mirror IMX, and end mirror EMX, as shown in equation 3.

$$C_{\text{configuration}} = \begin{pmatrix} \sigma_{\text{QPD1}}^{\text{IMX}} & \sigma_{\text{QPD1}}^{\text{EMX}} \\ \sigma_{\text{QPD2}}^{\text{IMX}} & \sigma_{\text{QPD2}}^{\text{EMX}} \end{pmatrix} \quad (3)$$

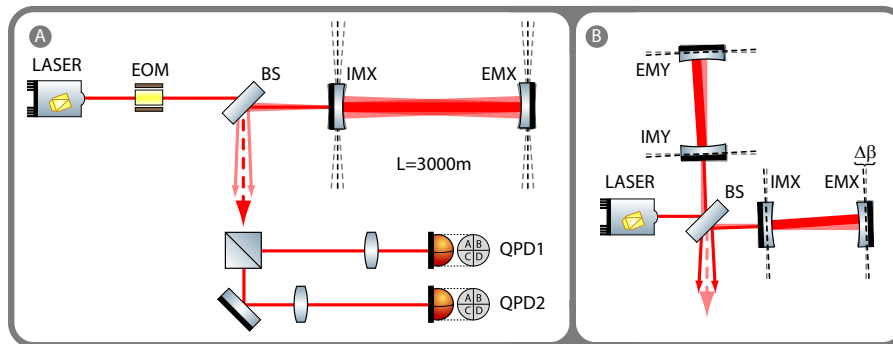


**Figure 2.** Two optical layouts used in the alignment analysis simulations. **(A)** shows the single arm cavity alignment control scheme investigated, and **(B)** shows the differential misalignment of arm cavities, for which coupling into dark port power was analysed.

The resulting control matrices for each of the three cavity configurations were as follows:

$$C_{LG_{00}^{small}} = \begin{pmatrix} 5.6152 & 0.0477 \\ 2.1607 & 3.5878 \end{pmatrix} = 5.6152 \begin{pmatrix} 1 & 0.009 \\ 0.385 & 0.639 \end{pmatrix} \quad (4)$$

$$C_{LG_{33}} = \begin{pmatrix} 7.444 & 0.022 \\ 2.741 & 4.771 \end{pmatrix} = 7.444 \begin{pmatrix} 1 & 0.003 \\ 0.368 & 0.641 \end{pmatrix} \quad (5)$$

$$C_{LG_{00}^{large}} = \begin{pmatrix} 17.774 & 15.330 \\ 11.472 & 2.725 \end{pmatrix} = 17.774 \begin{pmatrix} 1 & 0.862 \\ 0.645 & 0.153 \end{pmatrix}. \quad (6)$$

An ideal control matrix would be diagonal, since the off diagonal elements correspond to the presence of information from the unwanted mirror in a given photodetector signal. In this respect, the  $LG_{33}$  and  $LG_{00}^{small}$  configurations give control matrices which are much closer to the ideal than the  $LG_{00}^{large}$  configuration; the information from the two mirrors is better separated in these two configurations.

The next aspect of the interferometric performance of the  $LG_{33}$  mode to be investigated was the coupling of differential arm cavity misalignment to power at the interferometer output port. If the two arm cavities are differentially misaligned, the overlap of the two beams at the central beam splitter will not be complete, leading to a change in the light power present at the output port of the interferometer, as illustrated in panel **(B)** of figure 2. If this differential misalignment varies with time, the power measured at the dark port will also vary with time, producing a signal at the photodetector that is indistinguishable from gravitational wave signals. We obtained values for the output power enhancement due to differential misalignment for each of the three previously described cavity configurations, as shown in figure 3. Comparing the simulation results with the reference limit (around  $7 \times 10^{-9}$  W) calculated from a differential arm length requirement of  $10^{-15}$  m [14] and a dark fringe offset of  $10^{-12}$  m [15], we see that the  $LG_{00}^{small}$  configuration performs best, but crucially that the  $LG_{33}$  configuration also outperforms the  $LG_{00}^{large}$  configuration. In summary, for all the interferometric performance aspects analysed, the  $LG_{33}$  configuration performs significantly better than the  $LG_{00}^{large}$  configuration. The  $LG_{00}^{small}$  performs as well or better than the  $LG_{33}$  configuration, but it should be recalled that this will have a significantly higher thermal noise level, and for this reason is not representative of a likely configuration for advanced detectors.

The final comparison between the performance of the  $LG_{00}$  and  $LG_{33}$  modes was in terms of the overall detector sensitivity. Several scenarios for using the  $LG_{33}$  mode in Advanced Virgo detector were evaluated in [16], but here we just discuss a scenario which compares the

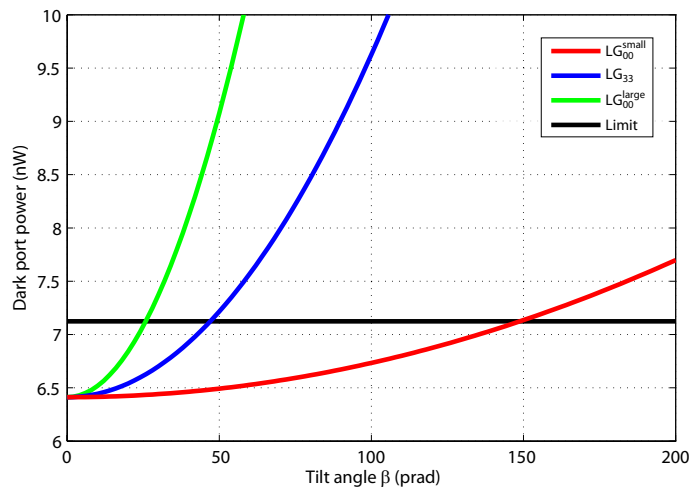


**Figure 3.** Dark port power as a function of differential arm cavity misalignment for the three different configurations. The black line shows the limit calculated for dark port power based on a differential arm length requirement of  $10^{-15}$  m for a dark fringe offset of  $10^{-12}$  m.

sensitivity of the detector with  $LG_{00}^{\text{large}}$  and  $LG_{33}$  modes, where both beams experience a 1 ppm clipping loss at the cavity mirrors. The cavity mirror curvatures, RoC, and beam sizes at the mirrors,  $w$ , for the two configurations in this scenario are shown in table 1. In each case the detector sensitivity was calculated using a version of Gravitational Wave Interferometer Noise Calculator (GWINC) [17] especially adapted for Advanced Virgo. Table 1 shows the results of the calculation for the two cases NS/NS, and BH/BH where the signal recycling detuning (SR det.) [18] was optimized for detection of signals from binary neutron star inspirals and binary black hole inspirals respectively. The figures of merit chosen were the effective detection ranges for the two signal sources,  $\Gamma_{\text{NS/NS}}$  and  $\Gamma_{\text{BH/BH}}$ . According to these results, the  $LG_{33}$  mode provides a relative improvement of the inspiral ranges by around 20% and 25% for signal recycling detunings of 750 Hz and 300 Hz respectively, compared to the  $LG_{00}$  mode. This corresponds to a potential increase by up to a factor of 2 in the observable event rate of the Advanced Virgo detector by using the  $LG_{33}$  mode instead of the  $LG_{00}$  mode. The method and results of the investigation described in this section are presented in more detail in [16].

Laser mode	SR det. [Hz]	$w$ [cm]	$l_{\text{clip}}$ [ppm]	RoC [m]	$\Gamma_{\text{NS/NS}}$ [Mpc]	$\Gamma_{\text{BH/BH}}$ [Mpc]
$LG_{00}^{\text{large}}$	750	6.47	1	1523	126	900
$LG_{33}$	750	3.94	1	1708	148	1140
$LG_{00}^{\text{large}}$	300	6.47	1	1523	130	580
$LG_{33}$	300	3.94	1	1708	163	715

**Table 1.** Relevant parameters and results of the GWINC simulation analysis of an Advanced Virgo design which considers identical clipping loss  $l_{\text{clip}}$  of 1 ppm at the arm cavity mirrors for both the  $LG_{00}^{\text{large}}$  and  $LG_{33}$  modes.

### 3. Table-top demonstrations

Following the positive results of the simulation investigation into the interferometric performance of the  $LG_{33}$  mode, we proceeded to perform table-top experiments to verify these results. The

first step was to generate LG modes with a reasonably high purity for use in the experiments. This was achieved using a Holoeye liquid-crystal on Silicon spatial light modulator (SLM), as for example in [19]. Upon reflection from the surface of the SLM, a beam can be imprinted with a transverse phase pattern determined by the user. By choosing the phase pattern to be that of a  $LG_{33}$  mode, i.e. three azimuthal phase vortices and three radial phase jumps of  $\pi$  for the helical case, one can achieve a partial conversion from the  $LG_{00}$  mode to the  $LG_{33}$  mode.

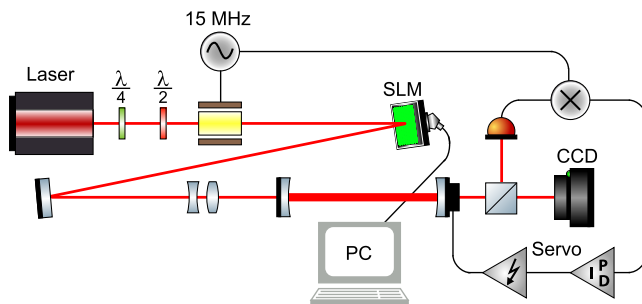


**Figure 4.** The experimental setup for mode cleaning a SLM generated higher-order LG beam. The input beam is converted to a higher-order LG beam by the SLM, then passed via a mode-matching telescope into the linear mode cleaner cavity. The transmitted light is used to generate an error signal which is fed back to the PZT attached to the curved end mirror to control the length of the cavity, and simultaneously imaged on the CCD camera.

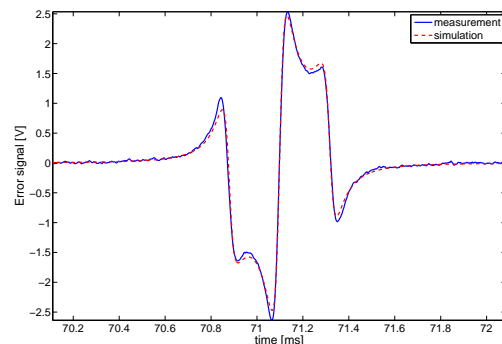


**Figure 5.** The blue trace and the red dashed trace show the measured sinusoidal  $LG_{33}$  beam and simulated  $LG_{00}$  PDH error signal respectively, for the linear mode cleaner cavity set up as shown in figure 4. The primary features are identical, as predicted in [16].

The experimental setup shown in figure 4 was then used to investigate the length control signals that could be generated for the resulting beam. The 1064 nm laser light was passed through an EOM to add 15 MHz sidebands to the light, for generating the PDH error signal for length control of the mode cleaner cavity. The light was then partially converted to the  $LG_{33}$  mode by interaction with the SLM, and passed into the mode cleaner cavity via a mode matching telescope. The light transmitted through the mode cleaner cavity was simultaneously measured with a photodiode and a CCD camera. The photodiode signal was mixed down with the 15 MHz signal to give the required error signal, which was then fed back to a Piezo-electric transducer attached to one of the mode cleaner mirrors, via two amplifier stages. In this way the length of the cavity was controlled to keep it in the resonant condition for any given mode order. The CCD measurement of the transmitted beam was then used for analysing the mode purity. The mode cleaner is a 2 mirror flat-concave cavity of length 21 cm and with a measured finesse of 172.

We verified the first result of the initial simulations by recording the PDH error signal generated using the  $LG_{33}$  mode, shown in figure 5. This signal was equivalent for the  $LG_{33}$  and  $LG_{00}$  modes as predicted, and therefore allowed us to control the cavity on resonance for the order 9  $LG_{33}$  mode. Demonstrating robust and repeatable feedback control of an optical cavity was a significant step in validating the higher-order LG mode operation of interferometers.

Figure 6 shows the beams before and after transmission through the mode cleaner cavity. It is immediately apparent that the transmitted beams exhibit greater circular symmetry than the input beams, as would be expected due to the filtering out of other spatial modes. We used the CCD measurement of the transmitted beam intensity pattern to estimate its mode content. This required fitting the beam size parameter to calibrate the CCD, and subtracting

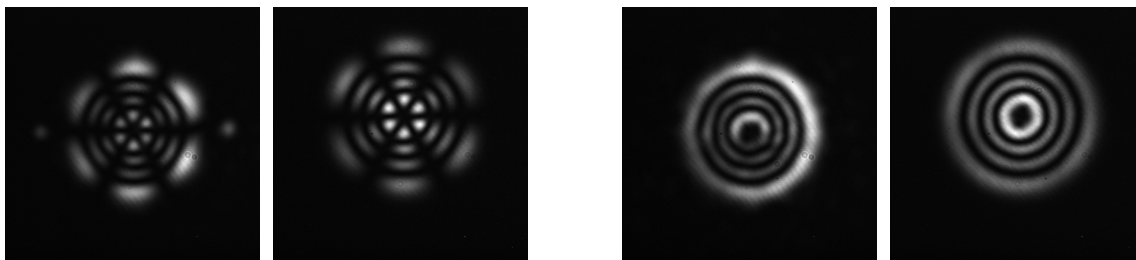


**Figure 6.** The measured intensity patterns of the sinusoidal (left pair) and helical (right pair)  $LG_{33}$  beams before (left of pairs) and after (right of pairs) transmission through the linear mode cleaner.

an ideal  $LG_{33}$  mode intensity pattern, with beam size given by the result of the fit, from the measured data. These residuals were then analysed by comparing the measured data with a numerical simulation of the setup which included some misalignment into the cavity, performed using the interferometer simulation Finesse [20]. For a Finesse model of the mode cleaner setup which included an input beam misalignment of  $-100 \mu\text{rad}$  in horizontal and  $60 \mu\text{rad}$  in vertical, the residual between the transmitted mode and an ideal  $LG_{33}$  matched the measured data extremely well. By performing a modal decomposition of the transmitted field in the simulation, we estimated the mode content of the transmitted beam, as shown in table 2. The

$u_{lp}^{\text{sin}}$ mode	3, 3	4, -1	2, -5	4, 1	2, 5	other
power	99%	0.4%	0.3%	0.1%	0.1%	< 10 ppm

**Table 2.** Results of a modal decomposition of the transmitted sinusoidal  $LG_{33}$  beam in the numerical model of the linear mode cleaner, with an input beam misalignment of  $-100 \mu\text{rad}$  in the horizontal axis, and  $60 \mu\text{rad}$  in the vertical axis. Most of the beam is in the sinusoidal  $LG_{33}$  mode, with the rest almost entirely found in other modes of order 9.

analysis showed that the transmitted beam was to 99 % in the  $LG_{33}$  mode for both the helical and sinusoidal cases. With an estimate of the transmitted mode purity, together with measurements of the cavity finesse and throughput efficiency, we were also able to estimate the  $LG_{33}$  mode content of the input beam to be 66 % for the helical beam, and 51 % for the sinusoidal beam. A detailed description of the method and results of this experiment can be found in [21].

#### 4. LG mode degeneracy investigation

One important difference between higher-order LG modes and the fundamental  $LG_{00}$  mode is that only the  $LG_{00}$  mode is unique in its mode order. For each higher-order mode there exists at least one other mode of the same order. Since the mode filtering effect of optical cavities relies principally on the round trip Gouy phase difference between different mode orders, they cannot therefore filter out all other modes than the  $LG_{33}$  when on resonance for order 9. For this reason we call the other order 9 modes degenerate with the  $LG_{33}$  mode.

This degeneracy of higher-order modes has serious implications for their application in gravitational wave interferometers. In the initial simulations reported in [16] the interferometer mirrors were modelled as perfect spherical curved mirrors. In reality however, the mirrors will have some small deviations from perfect spherical surfaces which can cause coupling from the  $LG_{33}$  mode into other modes of order 9. If we consider this process occurring within the arm



cavities of a gravitational wave interferometer, the degeneracy of the modes of order 9 will mean that the mode content of the circulating beam may have a significantly reduced proportion of  $LG_{33}$ , the remainder being made up principally of other order 9 modes. If the mode content of both arm cavities is different (which is likely to be the case if the coupling between modes is driven by the randomly oriented mirror surface distortions) the modal overlap at the beam splitter will be imperfect and the output port contrast will be reduced.

The method and results of a detailed numerical and analytical investigation into the effect of mirror surface distortions on the purity of LG modes within optical cavities were presented at this Amaldi meeting [22], and in [23], and another study on this topic is presented in [24]. One of the most important outcomes from the work described in [23] was the derivation of an analytical formula for predicting the amount of coupling between different LG modes upon reflection from a mirror, based on the spatial features of mirror surfaces as described by Zernike polynomial functions. In the limit that the height of the surface distortions is much smaller than the wavelength of the light, coupling between an incident mode  $LG_{pl}$  and a reflected mode  $LG_{p'l'}$  is only significantly caused by Zernike polynomials  $Z_n^m$  which satisfy the condition  $m = |l - l'|$ . Based on this result, it was possible to propose limits on the heights of the most important lower-order Zernike polynomial present on mirror surfaces, in order to achieve a circulating mode purity of over 99.9% [23].

## 5. Ongoing experimental investigations

Following the simulation studies and table-top experiments, we continue to pursue experimental tests of LG mode technology. Currently, this involves evaluating the performance of the  $LG_{33}$  mode in a suspended 10 m cavity at the Glasgow prototype facility, and the development of a high-power  $LG_{33}$  mode laser beam at the Hannover high-power laser facility.

Progression from table-top experiments to a prototype experiment with suspended mirrors is a standard feature of the development of new technologies for gravitational wave detectors, in order to ensure compatibility with realistic interferometer subsystems and requirements. Experiments at the Glasgow prototype also give us a way to investigate the LG mode degeneracy problem heretofore only looked at theoretically and numerically. Though we did not observe the detrimental effects of the mode degeneracy problem in our table-top experiment we believe this is most likely due to the relatively small beam sizes used on the mirrors, and the low cavity finesse in comparison to the advanced detector arm cavities. However, it is clear that LG modes must also work with larger beam sizes in order to provide the thermal noise benefits that make them attractive in the first place. LG modes must also be compatible with cavities of similar finesse to the advanced detector arm cavities. We have therefore been setting up an experiment at the Glasgow 10 m prototype facility which uses larger beam sizes in a higher finesse cavity.

In this experiment we will use an etched diffractive optic to facilitate the conversion from  $LG_{00}$  to  $LG_{33}$ , similar to that used in [25], rather than the SLM used in the table-top experiments. Though the SLM was very useful for prototyping purposes to investigate the effects of different phase profiles, a fixed transmissive optic allows to generate a higher mode purity with more stability than the SLM. The setup for the  $LG_{33}$  mode conversion bench is shown in figure 7. The beam is picked off from the previously used laser path (shown in purple) after a fibre output coupler, and directed with a flip mirror into the LG mode conversion area. The red path shows the  $LG_{33}$  mode conversion path, in which the beam passes through an EOM for generating the control sidebands, and the etched diffractive phaseplate. The resulting beam is then transmitted through a linear mode cleaner, which is feedback controlled using the PDH method to remain on resonance for mode order 9. This serves to increase the mode purity of the beam, as demonstrated in [21]. The transmitted beam is then passed back into the previously used laser path using another flip mirror, and on towards the suspended cavity. The green path is a phaseplate bypass path, which enables us to alternatively operate the linear mode cleaner

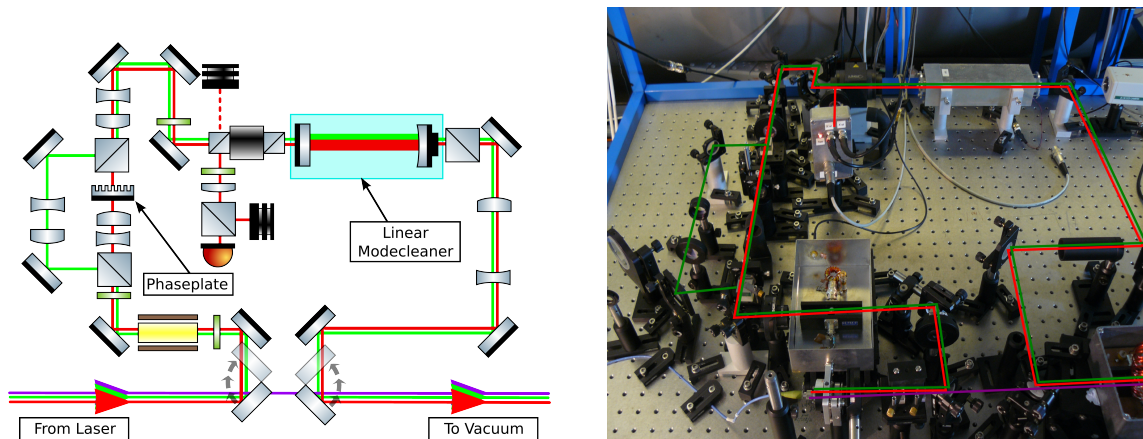


**Figure 7.** The laser mode conversion path on the Glasgow 10 m prototype input optics bench. The red line shows the  $LG_{33}$  mode path, and the green line shows the  $LG_{00}$  path that bypasses the phaseplate. The purple line shows the original  $LG_{00}$  laser path.

with the  $LG_{00}$  mode. Since the light transmitted by the mode cleaner must be defined by the cavity eigenmodes, the transmitted  $LG_{00}$  and  $LG_{33}$  beams should have the same alignment and mode matching relative to the suspended cavity. This enables us to make a valid assessment of the relative performance of the two modes within the suspended cavity.

The experimental work on LG modes at the Glasgow prototype is still under way, though we will soon have results about the performance of the  $LG_{33}$  mode within a cavity of finesse in the region of 600 - around the same finesse foreseen for the advanced detector arm cavities. We plan to analyse the length control signals for the cavity, as well as the transmitted beam intensity pattern, in order to ascertain the level of coupling between LG modes that occurs in the cavity. Analysis of the circulating mode purity, together with measured data of the cavity mirror surfaces, should enable us to verify the results of the theoretical investigation into the LG mode degeneracy problem described in [23]. With this information, we should be in a position to make well informed decisions on the suitability of LG mode technology for future detectors, based on the surface quality of the available optics.

Another crucial requirement for LG mode technology to be useful in future detectors is the ability to generate high-power and high-purity LG mode laser beams for the interferometer input. It is planned to use laser powers in excess of 100 W in the advanced detectors in order to bring the shot noise level down, so any prospective LG mode light source must also be able to reach comparable power levels. In collaboration with the members of the AEI in Hannover that developed the new 200 W laser system for Advanced LIGO [26], we are currently setting up an experiment to investigate the technical challenges of generating LG modes at such high powers. High-power beams from tens to hundreds of Watts will be passed through etched diffractive phaseplates. Following the example of our very first experiment on LG modes described in section 3, the LG beams that are generated will be then filtered by means of a linear mode cleaner, and their subsequent purity analysed. This work is also still at a preliminary stage, but we expect to be able to report results in the near future.

## 6. Summary

We have investigated the suitability of higher-order LG mode technology for use in future gravitational wave interferometers for reducing the test mass thermal noise, from many different angles. An initial simulation study showed that the longitudinal and angular control performance

of the LG<sub>33</sub> mode in an Advanced Virgo-like interferometer was significantly better than the LG<sub>00</sub> mode with the same clipping losses at the cavity mirrors. It was also shown that increases in the observable event rates of Advanced Virgo by up to a factor of 2 could be gained by using the LG<sub>33</sub> mode in place of the LG<sub>00</sub> mode. Table-top experiments verified the equivalence of the LG<sub>33</sub> mode and LG<sub>00</sub> mode for PDH longitudinal control signal generation in an optical cavity, and demonstrated the mode cleaning of SLM generated LG<sub>33</sub> beams to reach a mode purity of over 99%. More detailed theoretical investigations into the effects of mirror surface distortions on LG mode purity within optical cavities led to the derivation of an analytical formula for the coupling between LG modes caused by specific mirror distortions. Using this formula, mirror specifications required for compatibility with the LG<sub>33</sub> mode were subsequently derived. We are currently engaged in a collaborative effort with the University of Glasgow to verify the results of these theoretical investigations, by means of experiment within the 10 m prototype facility in Glasgow. We are also currently investigating the feasibility of generating high-power and high-mode purity LG<sub>33</sub> beams at the Hannover high-power laser facility. Higher-order LG modes can potentially offer a significant improvement in the sensitivity of future gravitational wave interferometers: our research program will evaluate how much of that potential is likely to be realisable in practice.

### Acknowledgments

We thank B. Barr, A. Bell, S. Huttner, J. Macarthur, B. Sorazu and K. Strain for providing the opportunity and helping to perform the LG mode experiments at the Glasgow 10 m prototype, and we thank C. Bogan, P. Kwee and B. Willke for the same assistance in the high-power LG modes experiment in Hannover. This document has been assigned the LIGO document number LIGO-P1100146.

### References

- [1] G. M. Harry and the LIGO Scientific Collaboration, 2010 *Class. Quantum Grav.* **27** 084006
- [2] The Virgo Collaboration, 2009 *Tech. Rep.* VIR-027A-09
- [3] B. Abbott, *et al*, 2009 *Rep. Prog. Phys.* **72** 076901
- [4] F. Acernese and the VIRGO Collaboration, 2006 *Class. Quantum Grav.* **23** 635
- [5] S. Rowan, J. Hough, and D. Crooks, 2005 *Phys. Lett. A* **347**, 25
- [6] J-Y. Vinet, 2009 *Living Rev. Relativity* **12**, <http://www.livingreviews.org/lrr-2009-5>
- [7] E. D'Ambrosio, 2003 *Phys. Rev. D* **67**, 102004
- [8] M. Bondarescu, O. Kogan, and Y. Chen, 2008 *Phys. Rev. D* **78**, 082002
- [9] B. Mours, E. Tournefier, and J.-Y. Vinet, 2006 *Class. Quantum Grav.* **23**, 5777
- [10] A. Freise and M. Mantovani, 2004 *Tech. Rep.* VIR-NOT-EGO-1390-330
- [11] E. D. Black, 2001 *Am. J. Phys.* **69**, 79
- [12] E. Morrison, D. I. Robertson, H. Ward, and B. J. Meers, 1994 *Appl. Opt.* **33**, 5041
- [13] M. Mantovani and A. Freise, 2008 *J. Phys. Conf. Ser.* **122**, 012026
- [14] R. Adhikari, S. Ballmer, and P. Fritschel, 2008 *LIGO Report* No. LIGO-T070236-00-D
- [15] R. Abbott *et al*, 2008, *LIGO Report* No. LIGO-T070247-00-I
- [16] S. Chelkowski, S. Hild and A. Freise, 2009 *Phys. Rev. D* **79**, 122002
- [17] GWINC, <http://lhocds.ligo-wa.caltech.edu:8000/advligo/GWINC>
- [18] S. Hild, H. Grote, M. Hewitson, H. Lück, J.R. Smith, K.A. Strain, B. Willke, and K. Danzmann, 2007 *Class. Quantum Grav.* **24**, 1513
- [19] N. Matsumoto *et al*, 2008 *J. Opt. Soc. Am. A* **25**, 1642
- [20] A. Freise, G. Heinzl, H. Lück, R. Schilling B. Willke and K. Danzmann, 2004 *Class. Quantum Grav.*, **21**, S1067-S1074. Finesse simulation software and manual available at <http://www.gwoptics.org/finesse/>
- [21] P. Fulda, K. Kokeyama, S. Chelkowski and A. Freise, 2010 *Phys. Rev. D* **82**, 012002
- [22] C. Bond *et al*, this conference proceedings
- [23] C. Bond, P. Fulda, L. Carbone, K. Kokeyama, A. Freise, 2011 *Phys. Rev. D* **84**, 102002
- [24] T. Hong, J. Miller, H. Yamamoto, Y. Chen, R. Adhikari, 2011 *Phys. Rev. D* **84**, 102001
- [25] S. A. Kennedy, M. J. Szabo, H. Teslow, J. Z. Porterfield, and E. R. Abraham, 2002 *Phys. Rev. A* **66**, 043801
- [26] L. Winkelmann *et al*, 2011 *Appl. Phys. B* **102**, 529-538